

# 1 A theta rhythm in awake macaque V1 and V4 2 and its attentional modulation

3 **Georgios Spyropoulos<sup>1</sup>, Conrado A. Bosman<sup>2,3</sup>, Pascal Fries<sup>1,2</sup>**

4 <sup>1</sup>Ernst Strüngmann Institute (ESI) for Neuroscience in Cooperation with Max Planck Society,  
5 Deutschordenstraße 46, 60528 Frankfurt, Germany, <sup>2</sup>Donders Institute for Brain, Cognition and Behaviour,  
6 Radboud University Nijmegen, Kapittelweg 29, 6525 EN Nijmegen, Netherlands, and <sup>3</sup>Swammerdam Institute for  
7 Life Sciences, Center for Neuroscience, Faculty of Science, University of Amsterdam, Sciencepark 904, 1098 XH  
8 Amsterdam, Netherlands.

9 Correspondence should be addressed to Pascal Fries, Ernst Strüngmann Institute (ESI) for  
10 Neuroscience in Cooperation with Max Planck Society, Deutschordenstraße 46,  
11 60528 Frankfurt, Germany. E-mail: [pascal.fries@esi-frankfurt.de](mailto:pascal.fries@esi-frankfurt.de).

12 Number of pages: 22

13 Number of figures: 10

14 Number of words

- 15 • for abstract: 194
- 16 • for introduction: 637
- 17 • for discussion: 1381

18 The authors declare no competing financial interests.

19 Acknowledgements: PF acknowledges grant support by DFG (SPP 1665, FOR 1847, FR2557/5-  
20 1-CORNET), EU (HEALTH-F2-2008-200728-BrainSynch, FP7-604102-HBP, FP7-600730-  
21 Magnetodes), a European Young Investigator Award, NIH (1U54MH091657-WU-Minn-  
22 Consortium-HCP), and LOEWE (NeFF). The authors thank Jarrod Dowdall for help with  
23 microsaccade detection and Martin Vinck for helpful comments on the manuscript.

## 24 **Abstract**

25 Theta-rhythmic neuronal synchronization has been described in hippocampus and high-level  
26 visual areas. Recent studies suggest that theta in visual areas might originate in V1. We  
27 analyzed simultaneous electrocorticographic (ECoG) grid recordings of local field potentials  
28 from areas V1 and V4 of two macaque monkeys performing a selective visual attention task.  
29 We found a  $\approx 4$  Hz theta rhythm, which was strongest at sites showing visually induced gamma-  
30 band activity. This theta rhythm was coherent between V1 and V4, with a predominant  
31 V1-to-V4 Granger causal influence. Locally, theta phase was correlated with power in a narrow  
32 gamma-frequency band. These theta-rhythmic processes were reduced by selective attention  
33 to a visual stimulus contralateral to the recorded visual areas. This attentional effect was  
34 substantial, particularly compared to other reported effects of attention in area V1. We also  
35 investigated, whether microsaccades (MSs) play a role in the generation or attentional  
36 modulation of theta. Stratification of MS rate between attention conditions, or elimination of  
37 MS-affected data epochs left the main results essentially unchanged. Thus, we find an  
38 MS-independent theta rhythm in the visually driven part of V1, which rhythmically modulates  
39 local gamma and entrains V4, and which is strongly reduced by attention.

## 40 **Significance Statement**

41 Theta rhythms, around 3-8 Hz, have been found in many different parts of the brain. They are  
42 predominant in the rodent hippocampus, yet have also been described in neocortex, primarily  
43 in frontal and parietal areas in relation to executive functions. Here, we show a 4 Hz theta  
44 rhythm in awake macaque monkey area V4 and primary visual cortex. This theta rhythm was  
45 spatially coextensive with visually induced gamma-band activity, and gamma power was  
46 modulated by theta phase. The strength of theta and of theta-rhythmic gamma modulation  
47 was markedly reduced by selective attention. Theta rhythmicity has been observed in  
48 microsaccade sequences, and microsaccades influence early visual activity. Yet, removing (the  
49 effects of) microsaccades did not influence the results.

## 50 **Introduction**

51 Neuronal activity shows rhythmic structure in several characteristic frequency bands (Buzsáki,  
52 2006). These different rhythms have often been linked to areas and/or functions, in which  
53 they predominate (Keitel and Gross, 2016). The theta rhythm has primarily been described in  
54 high-level areas of awake mammalian brains in the context of higher cognitive functions. A  
55 particularly strong theta rhythm exists in rodent medial temporal lobe (MTL), in particular the  
56 hippocampus and entorhinal cortex (O'Keefe and Recce, 1993; Hafting et al., 2008). This theta  
57 is found during exploratory behavior, and has been implicated in episodic memory (Skaggs et  
58 al., 1996; Dragoi and Buzsáki, 2006; Jezek et al., 2011). A similar theta rhythm also exists in  
59 the MTL of non-human and human primates during virtual maze navigation (Kahana et al.,  
60 1999) and visual exploration (Killian et al., 2012; Jutras et al., 2013), and has been linked to  
61 episodic memory encoding (Rutishauser et al., 2010; Lega et al., 2012; Jutras et al., 2013) and  
62 working memory maintenance (Raghavachari et al., 2001; Axmacher et al., 2010).

63 Hippocampal theta is synchronized with a theta rhythm in prefrontal cortex (PFC) (Siapas et  
64 al., 2005; Sirota et al., 2008; Brincat and Miller, 2015). Theta in PFC and strongly connected  
65 structures like the anterior cingulate cortex (ACC) and the posterior parietal cortex has been  
66 described when subjects exert executive control (Debener et al., 2005; Womelsdorf et al.,  
67 2010; Phillips et al., 2014; Voloh et al., 2015; Hawellek et al., 2016; Babapoor-Farrokhran et  
68 al., 2017).

69 The theta rhythm in non-human primate PFC shows long-distance synchronization to a theta  
70 rhythm in area V4 (Lee et al., 2005; Liebe et al., 2012). This PFC-V4 theta-band synchronization  
71 and the V4 theta rhythm is pronounced during the delay period of a visual working memory  
72 task, that is, in the absence of visual stimulation. In inferotemporal cortex, a theta rhythm has  
73 been described that is phase-locked to stimulus onset (Rollenhagen and Olson, 2005).

74 A theta rhythm at 3-5 Hz has also been described in mid-level visual areas V4 and V5/MT  
75 during selective visual attention tasks. A study in macaque area MT reported that the power  
76 of high-frequency (30-120 Hz) LFP components is modulated by the phase of low-frequency  
77 (1-8 Hz) components, and that this modulation is reduced by attention to the visual stimulus  
78 activating the recorded neurons (Esghaei et al., 2015). A study in macaque area V4 showed  
79 spike-field and spike-spike coherence at 2-4 Hz and straddling the lower end of the spectrum  
80 (Fries et al., 2008). This local low-frequency synchronization was enhanced by visual  
81 stimulation; furthermore, it was reduced by attention in the absence of visual stimulation. A  
82 subsequent study reported that the 4 Hz phase of LFP in macaque V4 modulates the gamma-  
83 band synchronization between areas V4 and V1 (Bosman et al., 2012). Also theta-band  
84 Granger causality (GC) influences around 4 Hz between V1 and V4 are stronger in the  
85 feedforward direction (Bastos et al., 2015b). This suggests that a 4 Hz rhythm might emerge  
86 in area V1 and entrain higher areas. Interestingly, a previous study found that microsaccades  
87 (MSs) occur at a 3-4 Hz rhythm and lead to evoked responses and perturbations in local  
88 synchronization in both, areas V1 and V4 (Bosman et al., 2009). This MS-related V1 4 Hz  
89 rhythm temporally structures also the V1-V2 interaction by co-modulating respective gamma  
90 power and frequency (Lowet et al., 2016).

91 Thus, several studies suggest a theta rhythm in V1, by e.g. showing a theta modulation of V1-  
92 V4 or V1-V2 interactions. Here, we analyzed simultaneous LFP recordings from awake  
93 macaque V1 and V4. We investigated whether the respective LFP power and phase-locking  
94 spectra actually show theta peaks, how this is related to visually induced activity, whether  
95 local gamma-band power is modulated by theta phase, to which degree these theta-related  
96 phenomena are independent of MSs, and whether they are modulated by selective visual  
97 attention.

## 98 **Materials and Methods**

### 99 **Subjects, stimuli and task**

100 Two adult male macaque monkeys participated in this study. All procedures were in  
101 accordance with Dutch and European regulations for the protection of animals and were  
102 approved by the animal ethics committee of Radboud University Nijmegen (Netherlands). The  
103 data analyzed here have been (partially) used in previous studies (Bosman et al., 2012; Brunet  
104 et al., 2014a; Brunet et al., 2014b; Pinotsis et al., 2014; Bastos et al., 2015a; Bastos et al.,  
105 2015b; Brunet et al., 2015; Richter et al., 2015; Vinck et al., 2015; Lewis et al., 2016).

106 Stimuli and behavior were controlled by the software CORTEX (<http://dally.nimh.nih.gov>).  
107 Stimuli were presented on a CRT monitor at 120 Hz non-interlaced. When the monkey touched  
108 a bar, a gray fixation point appeared at the center of the screen. When the monkey brought  
109 its gaze into a fixation window around the fixation point (0.85 degree radius in monkey K;  
110 1 deg radius in monkey P), a pre-stimulus baseline of 0.8 s started. If the monkey's gaze left  
111 the fixation window at any time, the trial was terminated. The measured eye positions during  
112 correct trials used for analysis differed only by an average of 0.03 deg of visual angle between  
113 the two attention conditions. After the baseline period, two physically isoluminant patches of  
114 drifting sinusoidal grating appeared (diameter= 3 degrees, spatial frequency  $\approx$ 1 cycles/degree,  
115 drift velocity  $\approx$ 1 degree/s, resulting temporal frequency  $\approx$ 1 cycle/s, contrast= 100%). The two  
116 grating patches chosen for a given recording session always had equal eccentricity, size,  
117 contrast, spatial frequency and drift velocity. The two gratings always had orientations that  
118 were orthogonal to each other, and they had drift directions that were incompatible with a  
119 Chevron pattern moving behind two apertures, to avoid pre-attentive binding. In any given  
120 trial, one grating was tinted yellow, the other blue, with the color assigned randomly across  
121 trials. The yellow and blue colors were physically equiluminant. After 1-1.5 s (0.8-1.3 s in  
122 monkey P), the fixation point changed color to match the color of one of the two gratings,  
123 thereby indicating this grating as the relevant stimulus and the other as irrelevant. For each  
124 trial, two independent change times for the two stimuli were determined randomly between  
125 stimulus onset and 4.5 s after cue onset, according to a slowly rising hazard rate. If the relevant  
126 stimulus changed (before or after the irrelevant stimulus changed), and the monkey released  
127 the bar within 0.15-0.5 s thereafter, the trial was terminated and a reward was given. If the  
128 monkey released the bar at any other time, the trial was terminated without reward. The  
129 stimulus changes were small changes in the grating pattern, with the stripes undergoing a  
130 gentle bend. During the bend, the outer ends of the grating stripes lagged increasingly behind  
131 the center of the stripes, until the lag reached 0.1 degree at 75 ms after the start of the bend.  
132 Over the course of another 75 ms, the stripes straightened again.

133 Several sessions (either separate or after attention-task sessions) were devoted to the  
134 mapping of receptive fields (RFs), using 60 patches of moving grating. Receptive field positions  
135 were stable across recording sessions (Bosman et al., 2012).

## 136 **Neurophysiological recordings and signal preprocessing**

137 Neuronal recordings were made from two left hemispheres in two monkeys through a  
138 micromachined 252-channel electrocorticographic electrode array (ECoG) implanted  
139 subdurally. The details of the production and the electrochemical properties have been  
140 described in a separate paper (Rubehn et al., 2009). Briefly, ECoG grids were 10 micron thick  
141 polyimide foils with 0.3 micron thick Platinum electrodes and conductive lanes embedded.  
142 Electrodes had an exposed surface with a diameter of 1 mm and a center-to-center spacing of  
143 2-3 mm. Electrodes were arranged in lanes, and two neighboring lanes ran parallel on one  
144 “finger” of the polyimide foil (Bastos et al., 2015b). The structuring in separate fingers avoided  
145 wrinkling of the ECoG on the brain surface and subsequent pressure points. For ECoG  
146 implantation, a 6.5x4 cm craniotomy over the left hemisphere in each monkey was performed  
147 under aseptic conditions with isoflurane anesthesia. The dura was opened and the ECoG was  
148 placed directly onto the brain under visual control. Several high resolution photos were taken  
149 before and after placement of the ECoG for later coregistration of ECoG signals with brain  
150 regions. After ECoG implantation, both the bone and the dural flap were placed back and  
151 secured in place. After a recovery period of approximately three weeks, we started with  
152 neuronal recordings.

153 Signals obtained from the 252-electrode grid were amplified 20 times by eight Plexon  
154 headstage amplifiers (Plexon, USA), high-pass filtered at 0.159 Hz, low-pass filtered at 8 kHz  
155 and digitized at 32 kHz by a Neuralynx Digital Lynx system (Neuralynx, USA). LFP signals were  
156 obtained by low-pass filtering at 200 Hz and downsampling to 1 kHz. Powerline artifacts were  
157 removed by digital notch filtering. The actual spectral data analysis included spectral  
158 smoothing that rendered the original notch invisible.

## 159 **Data analysis**

160 *General.* All analyses were done in MATLAB (The MathWorks, USA) and using FieldTrip  
161 (Oostenveld et al., 2011) (<http://fieldtrip.fcdonders.nl>).

162 *Recording electrodes versus recording sites.* During recordings, all ECoG electrodes were  
163 referenced against one silver ball implanted epidurally over the other hemisphere. This  
164 common reference could lead to artifactual correlations between the signals of separate  
165 electrodes. Therefore, all metrics of interaction between distant groups of neurons, that is the  
166 pairwise phase consistency (PPC) and Granger causality (GC), were applied after removing the  
167 common reference by local bipolar differentiation. That is, the signals from two immediately  
168 neighboring electrodes were subtracted from each other. We refer to the ECoG contacts as  
169 “electrodes” and to the local bipolar derivations as “recording sites” or just “sites”. All analyses  
170 of local neuronal activity used directly the signals recorded from the electrodes, to minimize  
171 preprocessing and to minimize reduction in theta amplitude due to theta phase alignment  
172 between neighboring electrodes.

173 *Selection of electrodes and sites.* The ECoG grids provided dense coverage of dorsal V1, the  
174 superficial part of dorsal V2, dorsal V4 and posterior TEO (Bosman et al., 2012; Bastos et al.,  
175 2015b). For simplicity, we refer to V1 and V2 sites as V1, and to V4 and TEO sites as V4.  
176 Monkey K had 45 electrodes on V1, resulting in 40 bipolar sites, and 24 electrodes on V4,  
177 resulting in 19 sites. Monkey P had 72 electrodes on V1, resulting in 64 sites, and 26 electrodes  
178 on V4, resulting in 21 sites.

179 *Normalization of signals across electrodes and recording sessions.* Signal amplitude could vary  
180 across electrodes because several separate headstages were used. Furthermore, signal  
181 amplitude of a given electrode could vary across sessions, probably due to variable quality of  
182 contact to the cortical surface. To equalize the contribution of different electrodes and  
183 sessions, we applied a z-transform: For each electrode and session, the raw LFP signal was  
184 demeaned and divided by its standard deviation.

185 *Segmenting data into epochs.* Each successfully completed trial contained three periods: The  
186 pre-stimulus, the pre-cue and the post-cue period. The pre-stimulus period was the time  
187 between fixation onset and stimulus onset. During the pre-stimulus period, monkeys fixated  
188 on a fixation point on a gray screen, and there was no stimulus presented and no cue had been  
189 nor was presented during that time. The pre-cue period was the time between stimulus onset  
190 and cue onset. During the pre-cue period, monkeys kept fixation, the stimuli were  
191 continuously present, one tinted yellow the other blue, chosen randomly, and the fixation  
192 point had not yet assumed a color, and thereby the attentional cue had not been given. The  
193 post-cue period was the time between cue onset and target change. During the post-cue  
194 period, monkeys kept fixation, the stimuli were continuously present with their tints and the  
195 fixation point was tinted in one of these colors, thereby providing the attentional cue. On  
196 approximately half of the trials, the post-cue period contained a distracter change, and the  
197 data immediately following this event were excluded as explained below. The pre-stimulus,  
198 pre-cue and post-cue periods all were of variable length across trials. The spectral analysis was  
199 based on epochs of fixed lengths. Therefore, the described task periods were cut into non-  
200 overlapping epochs. We aimed at excluding data soon after events, like stimulus onset, cue  
201 onset and distracter change, to minimize effects of post-event transients and non-  
202 stationarities on the metrics of rhythmicity and synchronization. Therefore, periods were cut  
203 into non-overlapping epochs, starting from the end of the period and stopping, before an  
204 epoch would have included data less than 0.5 s after those events. In general, we cut epochs  
205 of 1 s length, to achieve a fundamental spectral resolution (Rayleigh frequency) of one Hertz.  
206 This was used for the analysis of PPC, GC and phase-amplitude coupling (PAC). The PAC  
207 analysis required the prior estimation of the power time course, for which we employed  
208 window lengths of  $\pm 2.5$  cycles per frequency. In this case, epochs were cut such that the power  
209 estimation windows excluded data less than 0.5 s after events. The estimation of power  
210 spectra was based on 1.6 s epochs, because theta peaks were visible but less conspicuous  
211 when 1 s epochs were used.



212 *Spectral estimation.* Epochs were Hann tapered and Fourier transformed. For the PAC analysis,  
213 the  $\pm 2.5$  cycle long windows were also treated in this way. For the analysis of the spatial  
214 correlation between theta power and stimulus induced gamma power, the gamma-power  
215 estimation used multitaper spectral estimation with seven tapers taken from the discrete  
216 prolate spheroidal sequence, defined on 0.5 s long epochs (Mitra and Pesaran, 1999).

217 *Robust regression.* We reduced the  $1/f^n$  background in power spectra by estimating the  $1/f^n$   
218 component and subtracting it. Specifically, for each electrode separately, we pooled attention  
219 conditions and fitted a line to the log-log power plot between 0.625 and 10 Hz, using robust  
220 regression as implemented in the MATLAB “robustfit” function with default settings. Robust  
221 regression uses an iterative procedure that lends less weight to data that are far from the  
222 fitted function. Subsequently, the fitted line was subtracted to obtain the power residuals.

223 *Pairwise phase consistency (PPC) and Phase-amplitude coupling (PAC).* Phase locking was  
224 quantified with the pairwise phase consistency (PPC) metric (Vinck et al., 2010). We used PPC  
225 both to quantify the locking between LFPs recorded from separate sites, and to quantify the  
226 locking between the LFP phase and its amplitude fluctuations, that is, the PAC (phase-  
227 amplitude coupling) (Scheffer-Teixeira and Tort, 2016). PPC is not biased by the number of  
228 epochs, whereas the more conventional coherence metric has that bias. Essentially, the PPC  
229 calculation proceeds in two steps. First, phases are estimated for the multiple epochs of the  
230 two signals, and the relative phases are calculated. The second step is the crucial step: In  
231 conventional coherence calculation, those relative phases are averaged, which leads to the  
232 bias by epoch number; in PPC calculation, all possible pairs of relative phases are formed, the  
233 cosines between those relative phases are determined and those cosine values are averaged.

234 To quantify PAC, we computed the PPC between the LFP at lower frequencies, the “phase-  
235 frequencies”, and the time-varying power at higher frequencies, the “amplitude-frequencies”.  
236 One-second long epochs of the raw LFP and of its time-varying power were Fourier  
237 transformed, and locking among the phase estimates at the phase-frequencies was quantified  
238 as the PPC across all available epochs. PAC can in general only be estimated for pairs of phase-  
239 and amplitude-frequencies, for which the amplitude frequency is higher than the phase  
240 frequency. In addition, the estimation of time-varying power entails low-pass filtering, and  
241 PAC can only be estimated for pairs of phase- and amplitude-frequencies, for which this low-  
242 pass frequency is above the phase frequency. Power is estimated on the basis of epochs and  
243 tapers of finite length. As described above, we chose epochs of  $\pm 2.5$  cycle length per  
244 frequency. In order to assess the resulting low-pass filtering, we applied the power estimation  
245 10000 times to a random Gaussian process of the same length as the data epochs, and  
246 determined the frequency, at which this low-pass filtering reduced the average power to less  
247 than 70% of the power in the passband. For example, for 50 Hz, this cutoff frequency was  
248 7.7 Hz. This procedure was applied for each amplitude frequency, and the PAC for this  
249 amplitude frequency was only considered up to the respective phase frequency. The excluded  
250 combinations of phase-frequencies and amplitude-frequencies are masked with black in the  
251 figures. The PAC results shown here use phase and power estimates from the same electrode.

252 We also calculated PAC by combining phase estimates from one electrode with power  
253 estimates of neighboring electrodes, and this left the results essentially unchanged.

254 *Granger causality.* We used the non-parametric estimation of Granger causality (Dhamala et  
255 al., 2008). For this, Fourier spectra were estimated as described above and entered into a non-  
256 parametric spectral matrix factorization (NPSF) as implemented in the FieldTrip toolbox.

257 *Statistical testing.* The confidence intervals shown for power and PPC spectra in Figure 1 were  
258 estimated with a bootstrap procedure (1000 bootstrap replications for power, 500 for PPC)  
259 (Efron and Tibshirani, 1994): Spectra were first averaged across electrodes (for power) or site  
260 pairs (for PPC), and subsequently, the bootstrap was performed across epochs. All statistical  
261 comparisons were based on non-parametric permutation and included corrections for the  
262 multiple comparisons made across frequencies. We illustrate the procedure for the  
263 comparison of power between the two attention conditions. The power difference between  
264 the attention conditions was first averaged over all electrodes per monkey and then over the  
265 two animals, giving the observed power difference per frequency. Subsequently, the following  
266 procedure was done 1000 times: 1) The attention conditions were randomly exchanged  
267 between epochs, keeping the original number of epochs per attention conditions constant;  
268 2) The average power difference was calculated as described for the observed data; 3) The  
269 maximal (minimal) difference across all frequencies was placed into the randomization  
270 distribution of maximal (minimal) values; 4) The 2.5<sup>th</sup> percentile of the minimal values and the  
271 97.5<sup>th</sup> percentile of the maximal values were taken as statistical thresholds. The observed  
272 differences were compared to those thresholds. This procedure implements a non-parametric  
273 version of a two-sided test with multiple comparison correction (Nichols and Holmes, 2002).  
274 The same procedure was used for comparing power, PPC, GC and PAC values between  
275 attention conditions; for power and PAC, we used 1000 permutations, for PPC and GC 500  
276 permutations.

277 The spatial correlation coefficients and the PAC values were tested in two ways: They were  
278 compared between attention conditions as described, and they were additionally tested for  
279 the presence of significant correlation or PAC. In the case of PAC, the comparison was done  
280 between the observed values and a randomization distribution obtained by randomly pairing  
281 raw LFP epochs and power time courses 1000 times. After each random pairing and  
282 recalculation of PAC, maximal and minimal values across all frequency-frequency pairs were  
283 placed into the respective randomization distribution, and further testing proceeded as  
284 described. In the case of the spatial correlations, the comparison was done between the  
285 observed values and zero, because the Spearman rank correlation has no bias; the  
286 randomization was done by randomly pairing electrodes between the theta power residuals  
287 and the stimulus induced gamma. After each randomization, maximal and minimal correlation  
288 values across all tested frequencies were placed into the respective randomization  
289 distribution, and further testing proceeded as described.



290 *Microsaccade detection.* Raw vertical and horizontal eye position signals were low-pass  
291 filtered by replacing each value with the average over itself  $\pm 15$  samples (at 1 kHz sampling  
292 rate). Signals were then differentiated in time to obtain the vertical and horizontal velocities.  
293 Those are combined to obtain the eye speed irrespective of the direction of eye movement.  
294 Per trial, the standard deviation of eye speed was determined, and any deviation larger than  
295 5 SDs and lasting for at least 30 ms was considered a saccadic eye movement. Saccadic eye  
296 movements that remained within the fixation window were considered microsaccades (MSs).

297 *Stratification.* We intended to test, whether some of the observed differences in power, PPC  
298 or PAC between attention conditions were due to differences in the rate of MSs or in the  
299 power of theta, which existed between attention conditions. To this end, we used a  
300 stratification approach, that is, we randomly subsampled the available data to equate as well  
301 as possible the distributions of MS rates or theta power (Schoffelen et al., 2005). For MS  
302 stratification, we first calculated MS density by convolving the MS sequence with a Gaussian  
303 kernel with an SD of 150 ms (truncated at  $\pm 500$  ms). For each epoch, we calculated the average  
304 MS density, which was then used for stratification. Stratification for theta power was applied  
305 after removing the  $1/f^n$  component estimated by robust regression. Stratification for a given  
306 parameter (MS density or theta power) proceeded as follows: The parameter distributions  
307 were compiled for the two attention conditions and binned into 40 equally spaced bins. For  
308 each bin, the number of entries for the two attention conditions was equated by random  
309 subsampling with a procedure that aims at equating the parameter averages between the  
310 conditions as well as possible. This procedure is applied to the distributions per bin: 1) The  
311 condition with more entries is defined as the larger condition, the other as the smaller  
312 condition; 2) The mean of the parameter for the smaller condition is calculated and taken as  
313 target value; 3) The larger condition is randomly subsampled, by first drawing one entry at  
314 random, and then proceeding as follows: a) A further entry is randomly drawn; b) If the mean  
315 of the current bin entries (or the starter entry) is smaller (larger) than the target value, the  
316 new entry is added if it is larger (smaller), otherwise it is discarded and a new random draw is  
317 performed. This latter step aims at equating means; if no such entry is present, a randomly  
318 drawn entry is accepted.

## 319 **Results**

### 320 **Macaque areas V1 and V4 show a theta rhythm**

321 We first calculated power spectra averaged over all electrodes on V1 and V4 from periods,  
322 during which the monkey fixated and covertly monitored one of two simultaneously  
323 presented drifting grating stimuli (see Materials and Methods for the definition of  
324 “electrodes” versus “sites” and the attribution of electrodes and sites to areas). Those average  
325 power spectra exhibited clear peaks in the gamma and the beta range, with peak frequencies  
326 specific to each monkey; however, they did not exhibit clear peaks in the theta-frequency  
327 range (Fig. 1A,B). We have previously found that power spectra can fail to reveal rhythms that  
328 are nevertheless unequivocally detectable with metrics of phase locking (Vinck et al., 2013;

329 Brunet et al., 2014a). Here, we quantified phase locking by means of the pairwise phase  
330 consistency metric (PPC, see Materials and Methods). We calculated PPC spectra averaged  
331 over all possible pairs of sites within and between V1 and V4. The average PPC spectra  
332 confirmed the gamma and beta peaks and in addition revealed clear theta peaks around 4 Hz  
333 (Fig. 1C,D). Thus, awake macaque visual cortex shows a distinct theta rhythm, when activated  
334 by a visual stimulus.

### 335 **Selective attention reduces theta**

336 Previous studies reported similar theta or low-frequency rhythms in awake macaque areas V4  
337 and MT, which were reduced by selective attention (Fries et al., 2001; Esghaei et al., 2015).  
338 Theta might be generated in those extrastriate areas, or it might alternatively emerge already  
339 at earlier stages of the visual system. A previous study has found that Granger-causality  
340 between visual areas in the theta band is stronger in the feedforward than feedback direction  
341 (Bastos et al., 2015b). Thus, theta in extrastriate cortex might actually be driven by theta in  
342 primary visual cortex. Therefore, we investigated the theta rhythm separately in areas V1 and  
343 V4, and we tested if it was affected by selective attention. Raw power spectra averaged over  
344 all V1 electrodes showed a shallow bump around 4 Hz (Fig. 2A). This V1 theta rhythm was  
345 reduced when attention was directed to the contralateral visual stimulus, which was driving  
346 part of the V1 electrodes. A similar pattern was found in V4: There was a very shallow bump  
347 with an attentional reduction close to 4 Hz (Fig. 2B).

348 To reduce the  $1/f^n$  component of the power spectrum, we estimated it by robust regression  
349 and subtracted it from the total power (Manning et al., 2009). We followed this approach and  
350 found that in the absence of attention, there were distinct peaks around 4 Hz in both V1 and  
351 V4 (Fig. 2C,D). Those peaks were reduced when attention was directed to the contralateral  
352 hemifield.

353 We also calculated low-frequency phase-locking (PPC) spectra separately for pairs of sites  
354 within V1 or V4 and between V1 and V4, and we investigated whether this phase locking is  
355 affected by selective attention. The PPC spectra showed theta peaks for pairs of sites within  
356 and between V1 and V4, and this theta-band PPC was reduced by attention (Fig. 3).

### 357 **Theta is spatially coextensive with visually induced gamma**

358 Because theta was modulated by attention, while attention was directed to visual stimuli, we  
359 next investigated whether theta was related to visually induced activity. The ECoG covered  
360 large parts of V1, corresponding to large parts of the representation of the lower right visual  
361 quadrant, from the fovea out to about six degrees of visual angle. This allowed us to test  
362 whether theta was coextensive with visually driven activity. A given ECoG electrode does not  
363 provide conventional spike recordings, yet it does provide gamma power enhancements  
364 selectively for particular stimulus positions, that is, gamma power enhancements with  
365 circumscribed receptive fields (RFs) (Bosman et al., 2012; Lewis et al., 2016). The electrodes  
366 over V1 had varying overlap with the employed grating patch, which resulted in a topographic

367 map of visually induced gamma-band power with a clear peak at the representation of the  
368 stimulus (Fig. 4A). When we calculated a corresponding topographic map of theta power (after  
369 robust regression of the  $1/f^n$  component and its removal), it also showed a clear spatial peak  
370 (Fig. 4B). We calculated the spatial correlation (Spearman rank correlation) between low-  
371 frequency components (power residuals) and visually induced gamma power, across  
372 electrodes, separately for V1 and V4, for each attention condition, and for each of the low  
373 frequency components up to 10 Hz. The resulting correlation spectra reveal that across the  
374 spatial extension of both V1 and V4, visually induced gamma is positively correlated with theta  
375 when attention is ipsilateral (Fig. 4C,D, blue lines). In addition, visually induced gamma is  
376 negatively correlated with power around 1-4 Hz when attention is contralateral, and in V4 also  
377 when attention is ipsilateral (Fig. 4C,D). To ensure that the correlations shown in Figure 4C, D  
378 are not due to broadband power correlations, the analyses used gamma from the pre-cue  
379 period and theta power from the post-cue period (both with visual stimulation), that is, from  
380 non-overlapping trial epochs. Results are essentially the same if the post-cue period is used  
381 for both (data not shown).

### 382 **Theta-band Granger causality is stronger in the feedforward direction and reduced by** 383 **attention**

384 The PPC analysis revealed clear theta peaks for the visually driven sites, and a previous study  
385 found theta-band GC between visual areas to be generally stronger in the feedforward  
386 direction (Bastos et al., 2015b). Therefore, we next investigated in detail the GC between V1  
387 and V4 in the low-frequency range and separately for the two attention conditions. Figure 5A  
388 shows the GC spectra averaged over all V1-V4 site pairs, pooled across both attention  
389 conditions, and separately for the feedforward (V1-to-V4; green line) and feedback (V4-to-V1;  
390 black line) directions. These GC spectra reveal clear theta peaks, and they confirm that GC is  
391 stronger in the feedforward than feedback direction. Figure 5B shows the feedforward GC  
392 spectra separately for the two attention conditions. It reveals that feedforward GC in the theta  
393 band is enhanced when attention is to the ipsilateral stimulus. Figure 5C shows that the same  
394 pattern of attention effects exists for the feedback GC.

### 395 **Theta-gamma phase-amplitude coupling and its attentional modulation**

396 Several previous studies have found that the theta phase modulates gamma power, that is,  
397 there is theta-gamma phase-amplitude coupling, or PAC (Bragin et al., 1995; Sirota et al., 2008;  
398 Axmacher et al., 2010; Voloh et al., 2015). One of those studies also reported that theta-  
399 gamma PAC in area MT is decreased with attention to the activating stimulus (Esghaei et al.,  
400 2015). We investigated whether the theta rhythm described above for V1 and V4 modulates  
401 gamma power, and whether this is affected by selective attention. As described above, we  
402 found that theta is spatially coextensive with visually induced gamma and reduced by  
403 attention. Therefore, to explore whether theta phase modulates gamma amplitude, we first  
404 selected conditions with maximal theta strength, that is, visual stimulation with a non-  
405 attended stimulus. Figure 6A shows for one example electrode the raw spectral power as a  
406 function of time relative to the theta trough. This reveals that the amplitude of visually

407 induced gamma-band power is modulated systematically by theta phase. Figure 6B shows the  
408 resulting PAC, averaged over all electrodes in V1 and V4, and over both attentional conditions.  
409 It reveals a distinct peak of PAC between theta phase and gamma power. We note that the  
410 theta-rhythmic modulation of gamma was most pronounced for the high-frequency end of  
411 the gamma band. In addition, this analysis reveals PAC between the phase around 1 Hz and  
412 power in several frequency bands; this 1 Hz component is likely related to the temporal  
413 frequency of the drifting gratings (see Materials and Methods).

414 Figure 7 shows PAC separately for areas V1 and V4 and for the two attention conditions. In  
415 V1, there was a PAC peak for phase-frequencies around 4 Hz (Fig. 7A,B). This theta-gamma  
416 PAC was strongly reduced by attention (Fig. 7C). There were additional significant PAC  
417 components at lower phase frequencies, which partly also showed significant attentional  
418 effects. As mentioned above, these slower components are likely related to the temporal  
419 frequency of the drifting gratings. In contrast to V1, V4 did not show significant theta-gamma  
420 PAC, and also no significant PAC difference between attention conditions (Fig. 7D-F).

#### 421 **Control for microsaccades**

422 It has previously been shown that theta-band rhythmicity is present in the sequence of  
423 microsaccades (MSs) (Bosman et al., 2009; Lowet et al., 2016). MSs cause a movement of the  
424 retinal image and an MS-related response in the LFP and the multi-unit activity (Bosman et al.,  
425 2009). MSs also modulate the strength of gamma-band activity (Bosman et al., 2009; Lowet  
426 et al., 2016). Thus, the MS rhythm may underlie both the theta rhythm and the theta-gamma  
427 PAC observed here. To investigate this, we detected MSs and excluded data recorded between  
428 MS onset and 0.5 s thereafter. This substantially reduced the amount of available data.  
429 Nevertheless, the main results remained essentially unchanged (Fig. 8): Low-frequency power  
430 spectra (after robust regression of  $1/f^n$  and removal) show theta peaks for attention ipsilateral,  
431 which are reduced by attention to the contralateral stimulus (Fig. 8A,B); PPC spectra show  
432 theta peaks for all cases (Fig. 8C-E), and significant attentional reduction; PAC in area V1 shows  
433 a peak for theta-band phase frequencies and gamma-band amplitude frequencies only when  
434 attention is directed to the ipsilateral stimulus (Fig. 8F,G,H). Note that excluding MSs  
435 eliminated PAC components with phase frequencies at the temporal frequency of the drifting  
436 gratings. This suggests that those components were due to entrainment of MSs to the grating  
437 cycle.

#### 438 **Control for microsaccade rate**

439 In addition, we performed an alternative control, by equating the MS rate, that is, the MS  
440 temporal density, between attention conditions. This specifically controls for potential  
441 MS rate differences between attention conditions. Figure 9A shows the cumulative  
442 distribution of MS rate over the respective number of data epochs (see Materials and Methods  
443 for MS rate estimation). MS rate actually differed between attention conditions. We therefore  
444 stratified the data (see Materials and Methods) to arrive at two equally sized sets of epochs

445 with an essentially equal distribution of MS rates (dashed lines in Fig. 9A). After stratification,  
446 all main results remained essentially unchanged (Fig. 9B-G).

#### 447 **Control for theta power**

448 Finally, we controlled for the possibility that the effects of attention on theta-gamma PAC  
449 were fully explained by the effects of attention on theta power. Specifically, theta power was  
450 enhanced with ipsilateral attention, which might enhance the sensitivity of theta-gamma PAC  
451 quantification, which might in turn fully explain the enhanced theta-gamma PAC with  
452 ipsilateral attention. To investigate this possibility, we stratified for theta power. Figure 10A  
453 illustrates the stratification for one example electrode. Figure 10 B shows the average V1 PAC  
454 difference between attention conditions after stratification, and demonstrates that the  
455 attentional reduction of theta-gamma PAC in V1 is not due to attention effects on theta  
456 power. Figure 10 C shows the same control analysis for V4, confirming the absence of an  
457 attention effect for the combination of theta-band phase frequencies and gamma-band  
458 amplitude frequencies. Both V1 and V4 show some attention effects for phase frequencies at  
459 the temporal frequency of the drifting gratings and for a few scattered combinations of phase  
460 and amplitude frequencies. Note that multiple comparison correction across phase- and  
461 amplitude frequencies was less stringent due to power stratification. The other attention  
462 contrasts, without power stratification, randomly assign an attention condition per trial, for  
463 all electrodes together. Stratification was done for each electrode separately, which required  
464 the random assignment of attention condition to be done also per electrode, which then leads  
465 to a less stringent multiple comparison correction. This likely explains some of the scattered  
466 significant PAC points.

#### 467 **Discussion**

468 We demonstrate the presence of a  $\approx 4$  Hz theta rhythm in awake macaque V4 and V1. This  
469 theta rhythm is present selectively in sites driven by the visual stimulus, such that the spatial  
470 map of theta co-extends with the map of visually induced gamma-band activity. In V1, theta  
471 rhythmically modulates local gamma-band activity and thereby most likely the gamma-  
472 associated local processing of visual information. Theta rhythms in V1 and V4 synchronize, and  
473 an analysis of GC reveals a predominant feedforward influence. Both, local and inter-areal  
474 theta-rhythmic synchronization are substantially reduced by selective attention to a visual  
475 stimulus contralateral to the recorded areas. While previous studies have described that MSs  
476 can occur at a similar rhythm and influence V1, V2 and V4, we found that exclusion of MS  
477 effects leaves all main theta-related observations essentially unchanged.

478 We were somewhat surprised to find that theta shows a clear spatial correlation or  
479 coextension with visually induced gamma-band power. There were reasons to assume that a  
480 putative theta rhythm might be global across visual cortex. Hippocampal recordings suggest  
481 that theta is global in this structure, travelling as a wave from dorsal to ventral parts (Lubenov  
482 and Siapas, 2009; Patel et al., 2012). Also, there is the general notion that slower rhythms are  
483 more global than faster rhythms (von Stein and Sarnthein, 2000; Buzsáki and Draguhn, 2004).



484 Yet, our finding of a spatially specific theta, which is coupled to gamma by spatial extension  
485 and also through PAC, is also in agreement with one previous study: Inter-areal GC influences  
486 in both theta and gamma are typically stronger in the anatomically defined feedforward than  
487 feedback direction (Bastos et al., 2015b).

488 The theta rhythms in V1 and V4 are reduced by selective attention to a contralateral stimulus.  
489 Attention effects are typically smaller in V1 than in higher visual areas (for otherwise  
490 comparable conditions). This holds for firing rates (Luck et al., 1997; Buffalo et al., 2010) and  
491 gamma-band synchronization (Buffalo et al., 2011). In fact, different studies in V1 have  
492 reported attentional increases (Buffalo et al., 2011), decreases (Chalk et al., 2010) or the  
493 absence of an effect (Bosman et al., 2012) on gamma-band synchronization. By contrast, the  
494 attentional effects on theta appeared to be of similar strength in V4 and V1, entailing an  
495 unusually strong attention effect for V1.

496 The PAC analysis showed theta-gamma coupling that peaked for an amplitude-frequency at  
497 the high-frequency end of the visually induced gamma band activity. Thus, theta-rhythmic  
498 modulation is most apparent for this high-frequency part of the overall gamma peak. This  
499 might reflect a physiological asymmetry or be related to signal-to-noise ratio. Physiologically,  
500 it is conceivable that the modulation is in fact stronger at the upper flank of the gamma peak  
501 than at the lower flank, which would be equivalent to an asymmetric broadening of the  
502 gamma peak towards higher frequencies. Alternatively, the gamma-band peak is modulated  
503 in its entirety, yet the PAC metric ends up larger for the upper than the lower flank, e.g.  
504 because the gamma peak is superimposed on unmodulated (or less modulated)  $1/f^n$  power. If  
505 we consider the  $1/f^n$  component of the power spectrum as noise, this noise is larger for the  
506 lower than the upper flank.

507 Similarly, it is interesting to investigate the precise frequency of the observed theta rhythm.  
508 The basic spectra of power (residuals) and phase locking show peaks close to 4 Hz. The analysis  
509 of spatial correlation between theta power and visually-induced gamma power shows a  
510 broader peak that includes 4 Hz, yet extends up to 8 Hz. This suggests that the underlying  
511 phenomenon might actually occupy this broader frequency range, with theta merely peaking  
512 at 4 Hz for the particular stimulus and task conditions used here. Whether other stimuli or  
513 tasks make theta in V1 and/or V4 shift in frequency is an interesting topic for further study. In  
514 any case, the 4-8 Hz range found in the spatial correlation analysis is an interesting link to the  
515 classical hippocampal theta, which occupies this range. Hippocampal theta in fact shifts in  
516 frequency, e.g. depending on running speed (Shin and Talmov, 2001; Geisler et al., 2007).

517 The mechanisms behind the observed visual cortical theta rhythm and its attentional  
518 modulation are not yet clear. The mechanisms underlying hippocampal theta have been  
519 studied in great detail (Colgin, 2013), and hippocampal theta is partly synchronized to  
520 neocortex, e.g. to entorhinal and prefrontal areas. It is conceivable that this theta  
521 synchronizes further to intermediate and lower visual areas, yet we deem it unlikely that this  
522 is the source of the theta observed here. Such a mechanism would most likely not generate



523 the spatial coextension between theta and gamma, and the predominant GC direction from  
524 V1 to V4, which we observed here. The present results place further constraints on potential  
525 mechanisms: The fact that removing MSs left the main results essentially unchanged suggests  
526 that theta in visual cortex does not merely reflect theta-rhythmic MSs. Rather, the clear spatial  
527 co-extension between theta power and visually induced gamma suggests a role for visually  
528 driven activity in theta generation.

529 Recent studies have shown that attention samples visual stimuli at a theta rhythm. When  
530 human subjects have to detect the appearance of a faint stimulus at a peripheral location,  
531 their detection performance is modulated by the phase of a 7-8 Hz rhythm with a maximum  
532 over frontal cortex (Busch and VanRullen, 2010). This might reflect an  $\approx 8$  Hz rhythmic  
533 attentional sampling. In support of this, three subsequent studies show that two  
534 simultaneously monitored stimuli are attentionally sampled in alternation, each at  $\approx 4$  Hz  
535 (Landau and Fries, 2012; Fiebelkorn et al., 2013; Landau et al., 2015). A further study estimated  
536 the temporal sampling frequency of attention, and found it to be around 7 Hz for a single  
537 attended stimulus, 4 Hz for two and 2.6 Hz for three (Holcombe and Chen, 2013). These  
538 numbers are consistent with a single attentional sampling mechanism that is multiplexed over  
539 the to-be-attended stimuli. Such a scenario would also explain theta-rhythmic modulations of  
540 firing rates in inferotemporal (IT) cortex during the presentation of two stimuli (Rollenhagen  
541 and Olson, 2005). When IT neurons respond to one stimulus, and a second stimulus is added  
542 onto the screen, firing rates start oscillating at  $\approx 4$  Hz in a way that suggests that attention is  
543 drawn to the newly presented stimulus and subsequently alternates between the two stimuli.  
544 At first glance, these results might seem to suggest that visual cortical theta should be stronger  
545 for the attended stimulus, in contrast to our findings. Yet, the fact that divided attention tasks  
546 reveal theta-rhythmic sampling does not mean that attended stimuli are affected by stronger  
547 theta-rhythmic modulation than non-attended stimuli. The mentioned recordings in IT  
548 showed strong theta rhythmicity when two stimuli were presented, but weaker theta  
549 rhythmicity when a single stimulus was presented and thereby received full attention. Based  
550 on these and the present results, we propose that attention is more sustained, yet still weakly  
551 theta rhythmic, at the attended location, and that it theta-rhythmically scans the space around  
552 it, to explore other stimuli. As a consequence, non-attended stimuli receive attentional  
553 processing benefits only when they are attentionally scanned, leading to relatively strong  
554 theta rhythmicity. This scanning hypothesis is consistent with theta-rhythmic modulations of  
555 detection performance when one location on an extended stimulus is attended, while another  
556 location on the same object is not attended: The non-attended location is consistently  
557 sampled at an 8 Hz rhythm, yet 90 degrees later in the 8 Hz cycle than the attended location  
558 (Fiebelkorn et al., 2013).

559 Future studies will need to investigate whether attentional control structures show an  $\approx 8$  Hz  
560 sampling rhythm that is coherent to the sampled stimulus representations in visual cortex. As  
561 mentioned above, the  $\approx 8$  Hz EEG component, whose phase predicts human detection  
562 performance, is strongest over frontal areas (Busch and VanRullen, 2010). Also, spike and LFP

563 recordings in macaque parietal cortex have recently revealed a similar theta rhythm (Phillips  
564 et al., 2014; Hawellek et al., 2016). If such theta-rhythmic top-down influences were to be  
565 found, it will be interesting to understand how they fit with the predominantly bottom-up  
566 directed theta influences observed between visual areas (Bastos et al., 2015b). One possibility  
567 is that control structures exert a theta-rhythmic perturbation on early and even primary visual  
568 cortex, which then percolates up through the hierarchy of visual areas.

569

## References

570

571 Axmacher N, Henseler MM, Jensen O, Weinreich I, Elger CE, Fell J (2010) Cross-frequency coupling supports multi-  
572 item working memory in the human hippocampus. *Proceedings of the National Academy of Sciences of*  
573 *the United States of America* 107:3228-3233.

574 Babapoor-Farrokhran S, Vinck M, Womelsdorf T, Everling S (2017) Theta and beta synchrony coordinate frontal  
575 eye fields and anterior cingulate cortex during sensorimotor mapping. *Nature communications* 8:13967.

576 Bastos AM, Litvak V, Moran R, Bosman CA, Fries P, Friston KJ (2015a) A DCM study of spectral asymmetries in  
577 feedforward and feedback connections between visual areas V1 and V4 in the monkey. *NeuroImage*  
578 108:460-475.

579 Bastos AM, Vezoli J, Bosman CA, Schoffelen JM, Oostenveld R, Dowdall JR, De Weerd P, Kennedy H, Fries P  
580 (2015b) Visual areas exert feedforward and feedback influences through distinct frequency channels.  
581 *Neuron* 85:390-401.

582 Bosman CA, Womelsdorf T, Desimone R, Fries P (2009) A microsaccadic rhythm modulates gamma-band  
583 synchronization and behavior. *The Journal of neuroscience : the official journal of the Society for*  
584 *Neuroscience* 29:9471-9480.

585 Bosman CA, Schoffelen JM, Brunet N, Oostenveld R, Bastos AM, Womelsdorf T, Rubehn B, Stieglitz T, De Weerd  
586 P, Fries P (2012) Attentional stimulus selection through selective synchronization between monkey  
587 visual areas. *Neuron* 75:875-888.

588 Bragin A, Jandó G, Nádasdy Z, Hetke J, Wise K, Buzsáki G (1995) Gamma (40-100 Hz) oscillation in the  
589 hippocampus of the behaving rat. *The Journal of neuroscience : the official journal of the Society for*  
590 *Neuroscience* 15:47-60.

591 Brincat SL, Miller EK (2015) Frequency-specific hippocampal-prefrontal interactions during associative learning.  
592 *Nature neuroscience* 18:576-581.

593 Brunet N, Vinck M, Bosman CA, Singer W, Fries P (2014a) Gamma or no gamma, that is the question. *Trends in*  
594 *cognitive sciences* 18:507-509.

595 Brunet N, Bosman CA, Roberts M, Oostenveld R, Womelsdorf T, De Weerd P, Fries P (2015) Visual cortical gamma-  
596 band activity during free viewing of natural images. *Cereb Cortex* 25:918-926.

597 Brunet NM, Bosman CA, Vinck M, Roberts M, Oostenveld R, Desimone R, De Weerd P, Fries P (2014b) Stimulus  
598 repetition modulates gamma-band synchronization in primate visual cortex. *Proceedings of the National*  
599 *Academy of Sciences of the United States of America* 111:3626-3631.

600 Buffalo EA, Fries P, Landman R, Liang H, Desimone R (2010) A backward progression of attentional effects in the  
601 ventral stream. *Proceedings of the National Academy of Sciences of the United States of America*  
602 107:361-365.

603 Buffalo EA, Fries P, Landman R, Buschman TJ, Desimone R (2011) Laminar differences in gamma and alpha  
604 coherence in the ventral stream. *Proceedings of the National Academy of Sciences of the United States*  
605 *of America* 108:11262-11267.

606 Busch NA, VanRullen R (2010) Spontaneous EEG oscillations reveal periodic sampling of visual attention.  
607 *Proceedings of the National Academy of Sciences of the United States of America* 107:16048-16053.

608 Buzsáki G (2006) *Rhythms of the brain*. Oxford ; New York: Oxford University Press.

609 Buzsáki G, Draguhn A (2004) Neuronal oscillations in cortical networks. *Science* 304:1926-1929.

610 Chalk M, Herrero JL, Gieselmann MA, Delicato LS, Gotthardt S, Thiele A (2010) Attention reduces stimulus-driven  
611 gamma frequency oscillations and spike field coherence in V1. *Neuron* 66:114-125.

612 Colgin LL (2013) Mechanisms and functions of theta rhythms. *Annual review of neuroscience* 36:295-312.

613 Debener S, Ullsperger M, Siegel M, Fiehler K, von Cramon DY, Engel AK (2005) Trial-by-trial coupling of concurrent  
614 electroencephalogram and functional magnetic resonance imaging identifies the dynamics of  
615 performance monitoring. *The Journal of neuroscience : the official journal of the Society for*  
616 *Neuroscience* 25:11730-11737.

617 Dhamala M, Rangarajan G, Ding M (2008) Estimating Granger causality from fourier and wavelet transforms of  
618 time series data. *Physical review letters* 100:018701.

619 Dragoi G, Buzsáki G (2006) Temporal encoding of place sequences by hippocampal cell assemblies. *Neuron*  
620 50:145-157.

621 Efron B, Tibshirani RJ (1994) *An introduction to the bootstrap*: CRC Press.

622 Esghaei M, Daliri MR, Treue S (2015) Attention Decreases Phase-Amplitude Coupling, Enhancing Stimulus  
623 Discriminability in Cortical Area MT. *Frontiers in neural circuits* 9:82.

- 624 Fiebelkorn IC, Saalmann YB, Kastner S (2013) Rhythmic sampling within and between objects despite sustained  
625 attention at a cued location. *Current biology : CB* 23:2553-2558.
- 626 Fries P, Reynolds JH, Rorie AE, Desimone R (2001) Modulation of oscillatory neuronal synchronization by selective  
627 visual attention. *Science* 291:1560-1563.
- 628 Fries P, Womelsdorf T, Oostenveld R, Desimone R (2008) The effects of visual stimulation and selective visual  
629 attention on rhythmic neuronal synchronization in macaque area V4. *The Journal of neuroscience : the*  
630 *official journal of the Society for Neuroscience* 28:4823-4835.
- 631 Geisler C, Robbe D, Zugaro M, Sirota A, Buzsáki G (2007) Hippocampal place cell assemblies are speed-controlled  
632 oscillators. *Proceedings of the National Academy of Sciences of the United States of America* 104:8149-  
633 8154.
- 634 Hafting T, Fyhn M, Bonnevie T, Moser MB, Moser EI (2008) Hippocampus-independent phase precession in  
635 entorhinal grid cells. *Nature* 453:1248-1252.
- 636 Hawellek DJ, Wong YT, Pesaran B (2016) Temporal coding of reward-guided choice in the posterior parietal  
637 cortex. *Proceedings of the National Academy of Sciences of the United States of America* 113:13492-  
638 13497.
- 639 Holcombe AO, Chen WY (2013) Splitting attention reduces temporal resolution from 7 Hz for tracking one object  
640 to <3 Hz when tracking three. *Journal of vision* 13:12.
- 641 Jezek K, Henriksen EJ, Treves A, Moser EI, Moser MB (2011) Theta-paced flickering between place-cell maps in  
642 the hippocampus. *Nature* 478:246-249.
- 643 Jutras MJ, Fries P, Buffalo EA (2013) Oscillatory activity in the monkey hippocampus during visual exploration and  
644 memory formation. *Proceedings of the National Academy of Sciences of the United States of America*  
645 110:13144-13149.
- 646 Kahana MJ, Sekuler R, Caplan JB, Kirschen M, Madsen JR (1999) Human theta oscillations exhibit task dependence  
647 during virtual maze navigation. *Nature* 399:781-784.
- 648 Keitel A, Gross J (2016) Individual Human Brain Areas Can Be Identified from Their Characteristic Spectral  
649 Activation Fingerprints. *PLoS biology* 14:e1002498.
- 650 Killian NJ, Jutras MJ, Buffalo EA (2012) A map of visual space in the primate entorhinal cortex. *Nature* 491:761-  
651 764.
- 652 Landau AN, Fries P (2012) Attention samples stimuli rhythmically. *Current biology : CB* 22:1000-1004.
- 653 Landau AN, Schreyer HM, van Pelt S, Fries P (2015) Distributed Attention Is Implemented through Theta-  
654 Rhythmic Gamma Modulation. *Current biology : CB* 25:2332-2337.
- 655 Lee H, Simpson GV, Logothetis NK, Rainer G (2005) Phase locking of single neuron activity to theta oscillations  
656 during working memory in monkey extrastriate visual cortex. *Neuron* 45:147-156.
- 657 Lega BC, Jacobs J, Kahana M (2012) Human hippocampal theta oscillations and the formation of episodic  
658 memories. *Hippocampus* 22:748-761.
- 659 Lewis CM, Bosman CA, Womelsdorf T, Fries P (2016) Stimulus-induced visual cortical networks are recapitulated  
660 by spontaneous local and interareal synchronization. *Proceedings of the National Academy of Sciences*  
661 *of the United States of America* 113:E606-615.
- 662 Liebe S, Hoerzer GM, Logothetis NK, Rainer G (2012) Theta coupling between V4 and prefrontal cortex predicts  
663 visual short-term memory performance. *Nature neuroscience* 15:456-462, S451-452.
- 664 Lowet E, Roberts MJ, Bosman CA, Fries P, De Weerd P (2016) Areas V1 and V2 show microsaccade-related 3-4-  
665 Hz covariation in gamma power and frequency. *The European journal of neuroscience* 43:1286-1296.
- 666 Lubenov EV, Siapas AG (2009) Hippocampal theta oscillations are travelling waves. *Nature* 459:534-539.
- 667 Luck SJ, Chelazzi L, Hillyard SA, Desimone R (1997) Neural mechanisms of spatial selective attention in areas V1,  
668 V2, and V4 of macaque visual cortex. *Journal of neurophysiology* 77:24-42.
- 669 Manning JR, Jacobs J, Fried I, Kahana MJ (2009) Broadband shifts in local field potential power spectra are  
670 correlated with single-neuron spiking in humans. *The Journal of neuroscience : the official journal of the*  
671 *Society for Neuroscience* 29:13613-13620.
- 672 Mitra PP, Pesaran B (1999) Analysis of dynamic brain imaging data. *Biophysical journal* 76:691-708.
- 673 Nichols TE, Holmes AP (2002) Nonparametric permutation tests for functional neuroimaging: a primer with  
674 examples. *Hum Brain Mapp* 15:1-25.
- 675 O'Keefe J, Recce ML (1993) Phase relationship between hippocampal place units and the EEG theta rhythm.  
676 *Hippocampus* 3:317-330.
- 677 Oostenveld R, Fries P, Maris E, Schoffelen JM (2011) FieldTrip: Open source software for advanced analysis of  
678 MEG, EEG, and invasive electrophysiological data. *Computational intelligence and neuroscience*  
679 2011:156869.

- 680 Patel J, Fujisawa S, Berényi A, Royer S, Buzsáki G (2012) Traveling theta waves along the entire septotemporal  
681 axis of the hippocampus. *Neuron* 75:410-417.
- 682 Phillips JM, Vinck M, Everling S, Womelsdorf T (2014) A long-range fronto-parietal 5- to 10-Hz network predicts  
683 "top-down" controlled guidance in a task-switch paradigm. *Cereb Cortex* 24:1996-2008.
- 684 Pinotsis DA, Brunet N, Bastos A, Bosman CA, Litvak V, Fries P, Friston KJ (2014) Contrast gain control and  
685 horizontal interactions in V1: A DCM study. *NeuroImage*.
- 686 Raghavachari S, Kahana MJ, Rizzuto DS, Caplan JB, Kirschen MP, Bourgeois B, Madsen JR, Lisman JE (2001) Gating  
687 of human theta oscillations by a working memory task. *The Journal of neuroscience : the official journal  
688 of the Society for Neuroscience* 21:3175-3183.
- 689 Richter CG, Thompson WH, Bosman CA, Fries P (2015) A jackknife approach to quantifying single-trial correlation  
690 between covariance-based metrics undefined on a single-trial basis. *NeuroImage* 114:57-70.
- 691 Rollenhagen JE, Olson CR (2005) Low-frequency oscillations arising from competitive interactions between visual  
692 stimuli in macaque inferotemporal cortex. *Journal of neurophysiology* 94:3368-3387.
- 693 Rubehn B, Bosman C, Oostenveld R, Fries P, Stieglitz T (2009) A MEMS-based flexible multichannel ECoG-  
694 electrode array. *Journal of neural engineering* 6:036003.
- 695 Rutishauser U, Ross IB, Mamelak AN, Schuman EM (2010) Human memory strength is predicted by theta-  
696 frequency phase-locking of single neurons. *Nature* 464:903-907.
- 697 Scheffer-Teixeira R, Tort AB (2016) On cross-frequency phase-phase coupling between theta and gamma  
698 oscillations in the hippocampus. *eLife* 5.
- 699 Schoffelen JM, Oostenveld R, Fries P (2005) Neuronal coherence as a mechanism of effective corticospinal  
700 interaction. *Science* 308:111-113.
- 701 Shin J, Talnov A (2001) A single trial analysis of hippocampal theta frequency during nonsteady wheel running in  
702 rats. *Brain research* 897:217-221.
- 703 Siapas AG, Lubenov EV, Wilson MA (2005) Prefrontal phase locking to hippocampal theta oscillations. *Neuron*  
704 46:141-151.
- 705 Sirota A, Montgomery S, Fujisawa S, Isomura Y, Zugaro M, Buzsáki G (2008) Entrainment of neocortical neurons  
706 and gamma oscillations by the hippocampal theta rhythm. *Neuron* 60:683-697.
- 707 Skaggs WE, McNaughton BL, Wilson MA, Barnes CA (1996) Theta phase precession in hippocampal neuronal  
708 populations and the compression of temporal sequences. *Hippocampus* 6:149-172.
- 709 Vinck M, van Wingerden M, Womelsdorf T, Fries P, Pennartz CM (2010) The pairwise phase consistency: A bias-  
710 free measure of rhythmic neuronal synchronization. *NeuroImage* 51:112-122.
- 711 Vinck M, Womelsdorf T, Buffalo EA, Desimone R, Fries P (2013) Attentional modulation of cell-class-specific  
712 gamma-band synchronization in awake monkey area V4. *Neuron* 80:1077-1089.
- 713 Vinck M, Hurdeman L, Bosman CA, Fries P, Battaglia FP, Pennartz CM, Tiesinga PH (2015) How to detect the  
714 Granger-causal flow direction in the presence of additive noise? *NeuroImage* 108:301-318.
- 715 Voloh B, Valiante TA, Everling S, Womelsdorf T (2015) Theta-gamma coordination between anterior cingulate  
716 and prefrontal cortex indexes correct attention shifts. *Proceedings of the National Academy of Sciences  
717 of the United States of America* 112:8457-8462.
- 718 von Stein A, Sarnthein J (2000) Different frequencies for different scales of cortical integration: from local gamma  
719 to long range alpha/theta synchronization. *International journal of psychophysiology : official journal of  
720 the International Organization of Psychophysiology* 38:301-313.
- 721 Womelsdorf T, Johnston K, Vinck M, Everling S (2010) Theta-activity in anterior cingulate cortex predicts task  
722 rules and their adjustments following errors. *Proceedings of the National Academy of Sciences of the  
723 United States of America* 107:5248-5253.
- 724
- 725

## 726 Legends

727 **Figure 1.** Average power and phase locking spectra for the two macaques. **A**, Average power  
728 spectrum of the ECoG LFP in V1 and V4, for monkey K, during attentional monitoring of a  
729 drifting grating. Data around the 50 Hz line-noise frequency and harmonics is not shown. **B**,  
730 Same as **A**, but for monkey P. **C**, Average phase locking (PPC) spectrum across all possible site  
731 pairs within and between V1 and V4, for monkey K. The shading (hardly visible behind the  
732 lines) shows the 95% confidence interval based on a bootstrap procedure across trials. **D**,  
733 Same as **C**, but for monkey P.

734 **Figure 2.** Average low-frequency LFP power spectra and their modulation by selective  
735 attention. **A**, Average LFP power spectra in area V1 with attention toward (red) and away  
736 (blue) from the activating stimulus. The gray-shaded region indicates frequencies with a  
737 significant difference between attention conditions ( $p < 0.05$ ; non-parametric permutation test  
738 with correction for multiple comparisons across frequencies). **B**, Same as **A**, but for area V4.  
739 **C**, Same as **A**, but showing the power residuals after removing the  $1/f^n$  component of the  
740 power spectrum through robust regression (see Materials and Methods). **D**, Same as **C**, but  
741 for area V4.

742 **Figure 3.** Average low-frequency LFP phase-locking (PPC) spectra and their modulation by  
743 selective attention. **A**, Average LFP phase locking between sites within area V1 with attention  
744 toward (red) and away from (blue) the activating stimulus. The gray-shaded region indicates  
745 frequencies with a significant difference between attention conditions ( $p < 0.05$ ; non-  
746 parametric permutation test with correction for multiple comparisons across frequencies). **B**,  
747 Same as **A**, but between sites within area V4. **C**, Same as **A**, but between sites in area V1 and  
748 sites in area V4.

749 **Figure 4.** The theta rhythm coextends with the visually induced gamma rhythm. **A**, Visually  
750 induced LFP gamma-band power, as a function of spatial location in V1 (indicated by blue  
751 outline) and V4 (indicated by green outline). **B**, Same as **A**, but showing LFP theta-band power  
752 after removing the  $1/f^n$  component. **C**, Correlation between 1) visually induced gamma-band  
753 power and 2) the power ( $1/f^n$  removed) at the frequency indicated on the x-axis, across  
754 recording sites in area V1. Colored lines on the bottom indicate frequencies with significant  
755 correlations with attention toward (red) or away from (blue) the activating stimulus ( $p < 0.05$ ;  
756 non-parametric permutation test with correction for multiple comparisons across  
757 frequencies). The gray line on the bottom indicates frequencies with a significant difference  
758 in correlation between the attention conditions (same test). **D**, Same as **C**, but for area V4.

759 **Figure 5.** Average low-frequency Granger causality (GC) spectra between V1 and V4 sites. **A**,  
760 Average GC-influence spectra between V1 and V4 in the feedforward (green) and feedback  
761 directions (black). The gray-shaded regions indicate frequencies with a significant difference  
762 between bottom-up and top-down ( $p < 0.05$ ; non-parametric permutation test with correction  
763 for multiple comparisons across frequencies). **B**, Average GC-influence spectra between V1  
764 and V4 in the feedforward direction, with attention toward (red) and away from (blue) the



765 activating stimulus. The gray-shaded regions indicate frequencies with a significant difference  
766 between attention conditions ( $p < 0.05$ ; non-parametric permutation test with correction for  
767 multiple comparisons across frequencies). Frequency regions with significant positive and  
768 negative attention effects were directly abutting to each other, and therefore the gray region  
769 is continuous. **C**, Same as **B**, but for the feedback direction.

770 **Figure 6.** Theta-gamma phase-amplitude coupling (PAC) in visual cortex. **A**, LFP power of one  
771 example site in the 50-150 Hz range (y-axis) as a function of time relative to the theta trough  
772 (x-axis). **B**, Grand-average PAC as a function of the frequency defining the power (y-axis) and  
773 the frequency defining the phase (x-axis). The semitransparent gray mask indicates frequency  
774 pairs with non-significant PAC ( $p < 0.05$ ; non-parametric permutation test with correction for  
775 multiple comparisons across frequency pairs). The black area indicates frequency pairs  
776 excluded from the analysis (see Materials and Methods).

777 **Figure 7.** Modulation of PAC by selective attention. **A, B**, Average PAC in area V1 with attention  
778 toward (**A**) and away from (**B**) the activating stimulus. **C**, Average PAC difference in area V1  
779 between the two attention conditions shown in **A** and **B**. The semitransparent gray mask  
780 indicates frequency pairs with non-significant PAC ( $p < 0.05$ ; non-parametric permutation test  
781 with correction for multiple comparisons across frequency pairs). The black area indicates  
782 frequency pairs excluded from the analysis (see Materials and Methods). **D, E, F**, Same as **A**,  
783 **B, C**, but for area V4.

784 **Figure 8.** Attention contrast, excluding epochs with microsaccades. **A**, Average LFP power  
785 spectra in area V1 after removing the  $1/f^n$  component, with attention toward (red) and away  
786 (blue) from the activating stimulus. **B**, Same as **A**, but for area V4. **C**, Average LFP phase locking  
787 between sites in area V1 and sites in area V4, with attention toward (red) and away from (blue)  
788 the activating stimulus. **D, E** Same as **C**, but for pairs of sites within area V1 (**D**) and area V4  
789 (**E**). **A-E**, The gray-shaded region indicates frequencies with a significant difference between  
790 attention conditions ( $p < 0.05$ ; non-parametric permutation test with correction for multiple  
791 comparisons across frequencies). **F, G**, Average PAC in area V1 with attention toward (**F**) and  
792 away from (**G**) the activating stimulus. **H**, Average PAC difference in area V1 between the two  
793 attention conditions. **F-H**, The semitransparent gray mask indicates frequency pairs with non-  
794 significant PAC ( $p < 0.05$ ; non-parametric permutation test with correction for multiple  
795 comparisons across frequency pairs). The black area indicates frequency pairs excluded from  
796 the analysis (see Materials and Methods).

797 **Figure 9.** Attention contrast, controlled for microsaccade (MS) rate. Same analyses as shown  
798 in Figure 8, but after equating the MS rate. **A**, Cumulative distribution of MS rate with  
799 attention toward (red) and away (blue) from the activating stimulus. Solid lines show data  
800 before stratification; dashed lines show data after stratification. Note that after stratification,  
801 the lines for the two attention conditions overlap essentially perfectly. **B**, Average LFP power  
802 spectra in area V1 after removing the  $1/f^n$  component, with attention toward (red) and away  
803 (blue) from the activating stimulus. **C**, Same as **B**, but for area V4. **D**, Average LFP phase locking

804 between sites in area V1 and sites in area V4, with attention toward (red) and away from (blue)  
805 the activating stimulus. **E, F**, Same as **D**, but for pairs of sites within area V1 (**E**) and area V4  
806 (**F**). **B-F**, The gray-shaded region indicates frequencies with a significant difference between  
807 attention conditions ( $p < 0.05$ ; non-parametric permutation test with correction for multiple  
808 comparisons across frequencies). **G**, Average PAC difference in area V1 between the two  
809 attention conditions. The semitransparent gray mask indicates frequency pairs with non-  
810 significant PAC ( $p < 0.05$ ; non-parametric permutation test with correction for multiple  
811 comparisons across frequency pairs). The black area indicates frequency pairs excluded from  
812 the analysis (see Materials and Methods).

813 **Figure 10.** Attention contrast, controlled for theta power. **A**, Example V1 LFP power spectrum  
814 with attention toward (red) and away from (blue) the activating stimulus. Solid lines show data  
815 before stratification; dashed lines show data after stratification. The gray bar at the bottom  
816 indicates statistical significance between the stratified spectra ( $p < 0.05$ ; non-parametric  
817 permutation test with correction for multiple comparisons across frequencies). **B**, Average  
818 PAC difference in area V1 between the two attention conditions. The semitransparent gray  
819 mask indicates frequency pairs with non-significant PAC ( $p < 0.05$ ; non-parametric permutation  
820 test with correction for multiple comparisons across frequency pairs). The black area indicates  
821 frequency pairs excluded from the analysis (see Materials and Methods). **C**, Same as **B**, but for  
822 area V4.

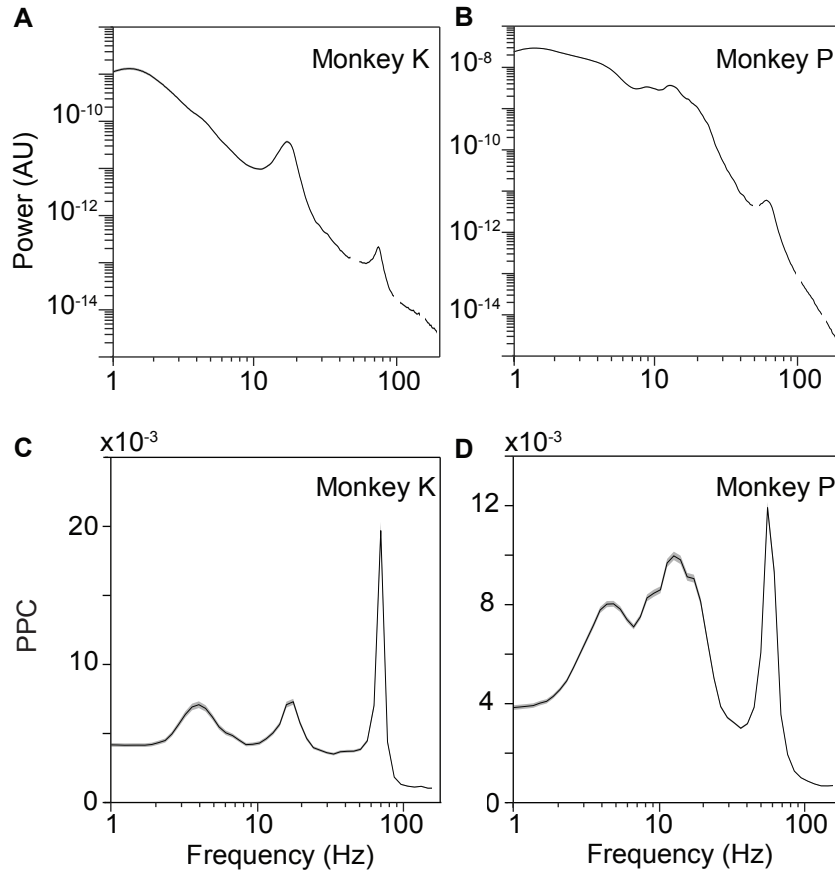


Figure 1  
Spyropoulos et al.

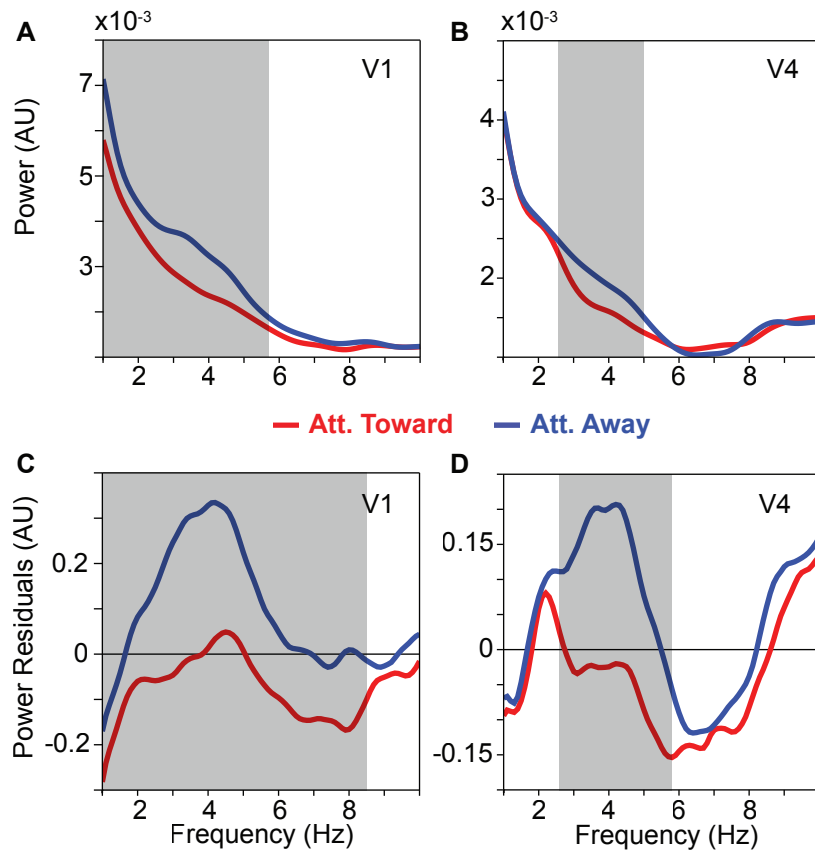


Figure 2  
Spyropoulos et al.

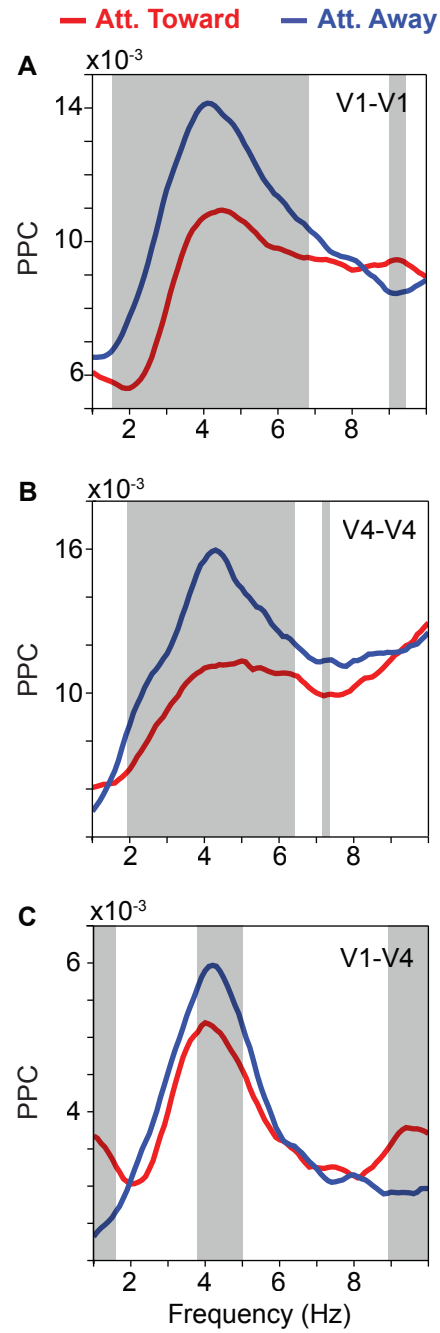


Figure 3  
Spyropoulos et al.

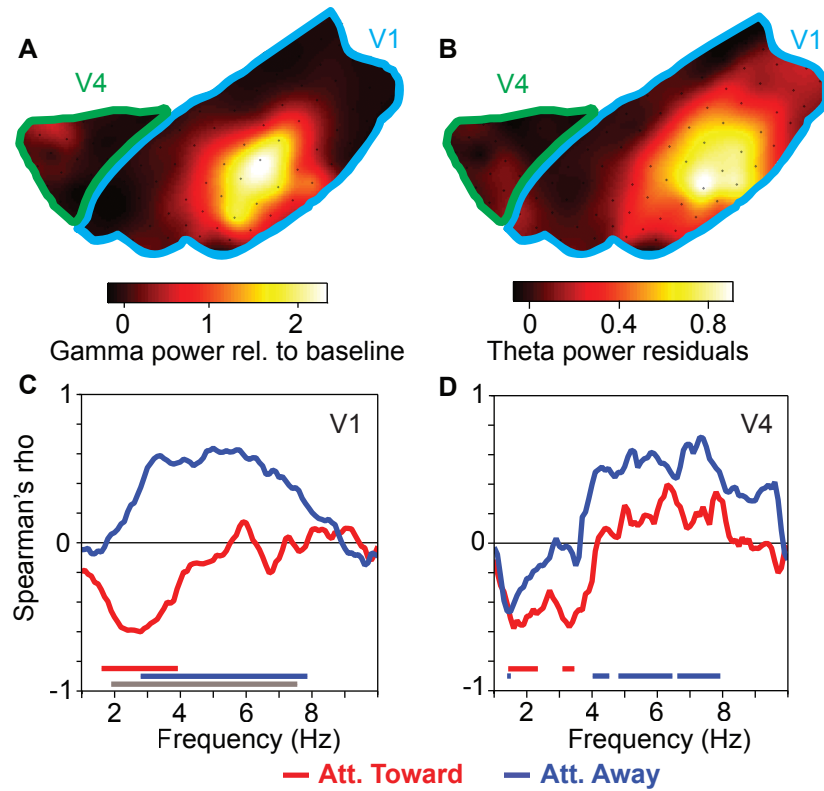


Figure 4  
Spyropoulos et al.



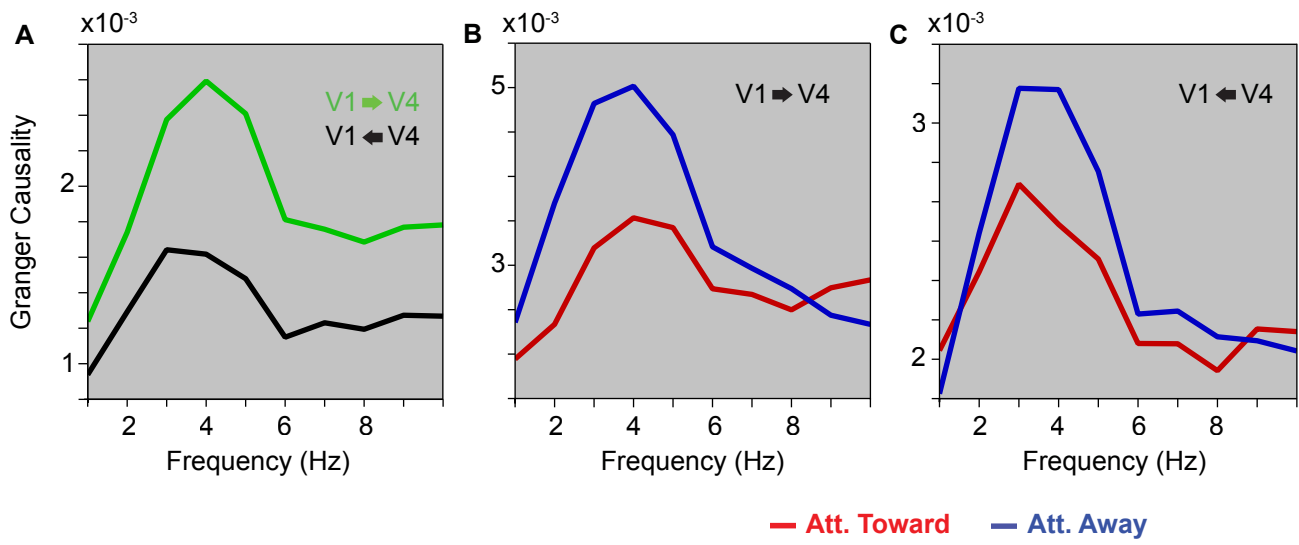


Figure 5  
Spyropoulos et al.

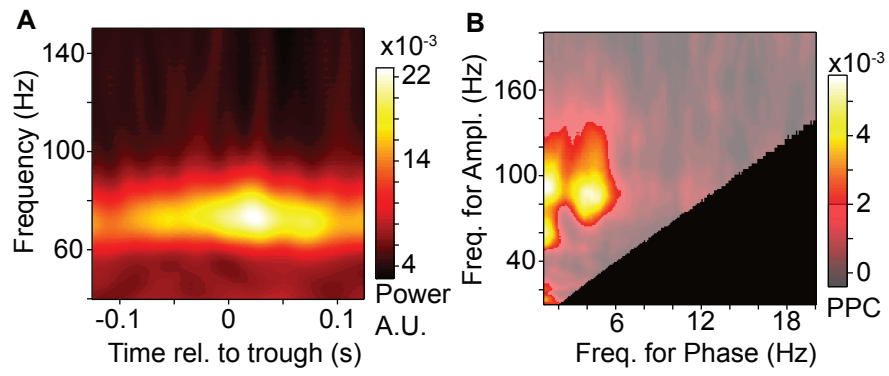


Figure 6  
Spyropoulos et al.

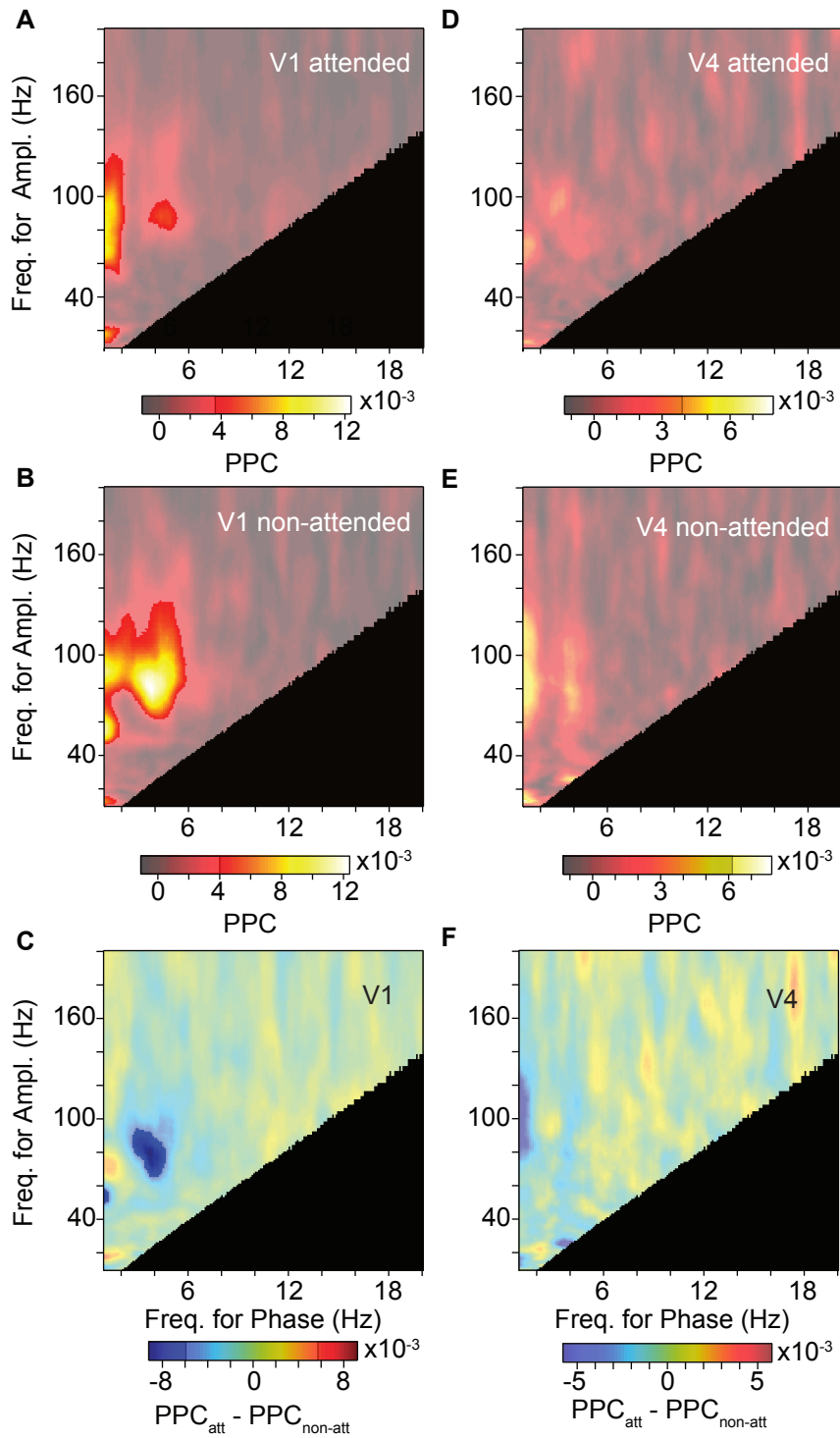


Figure 7  
Spyropoulos et al.

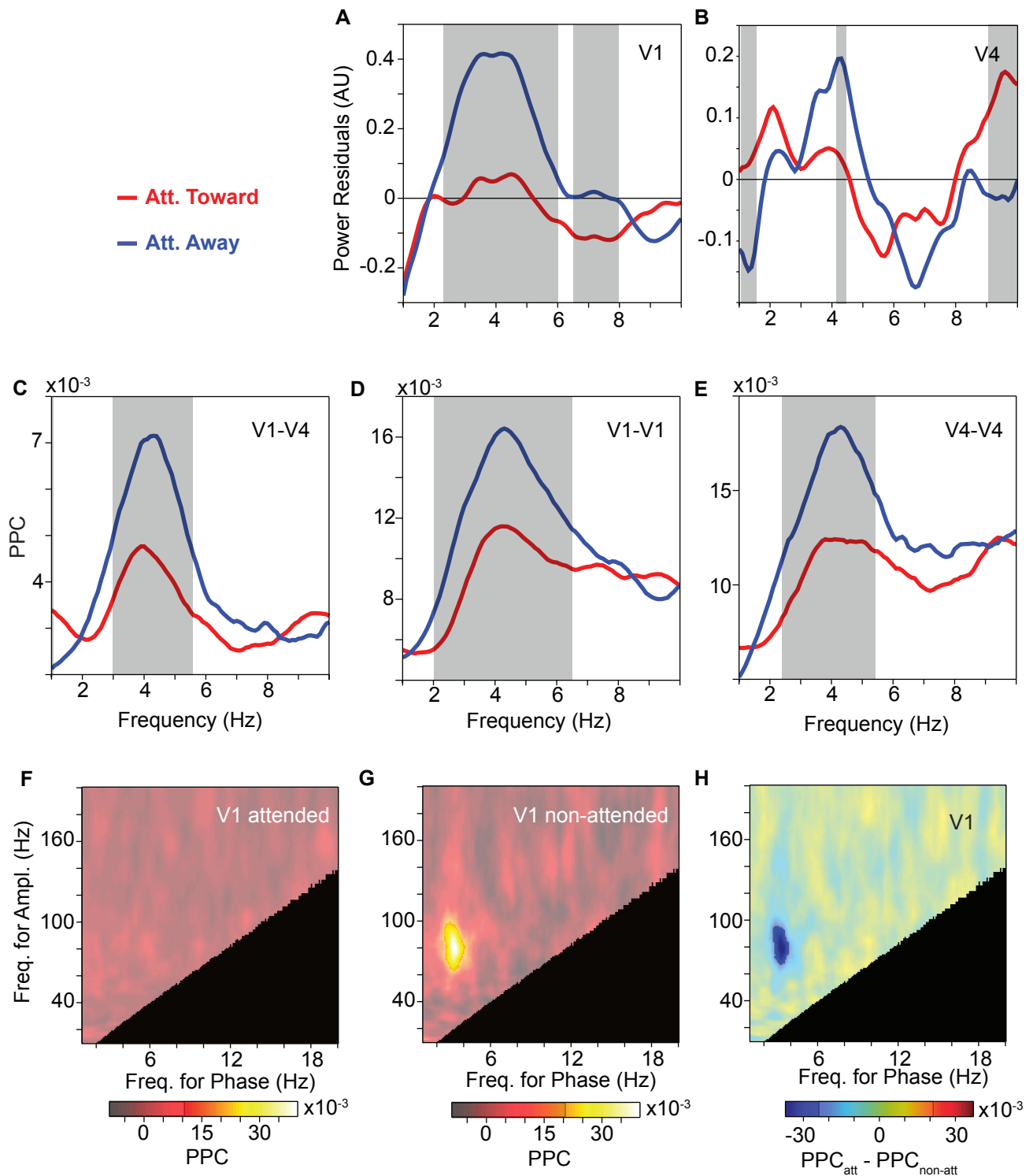


Figure 8  
Spyropoulos et al.

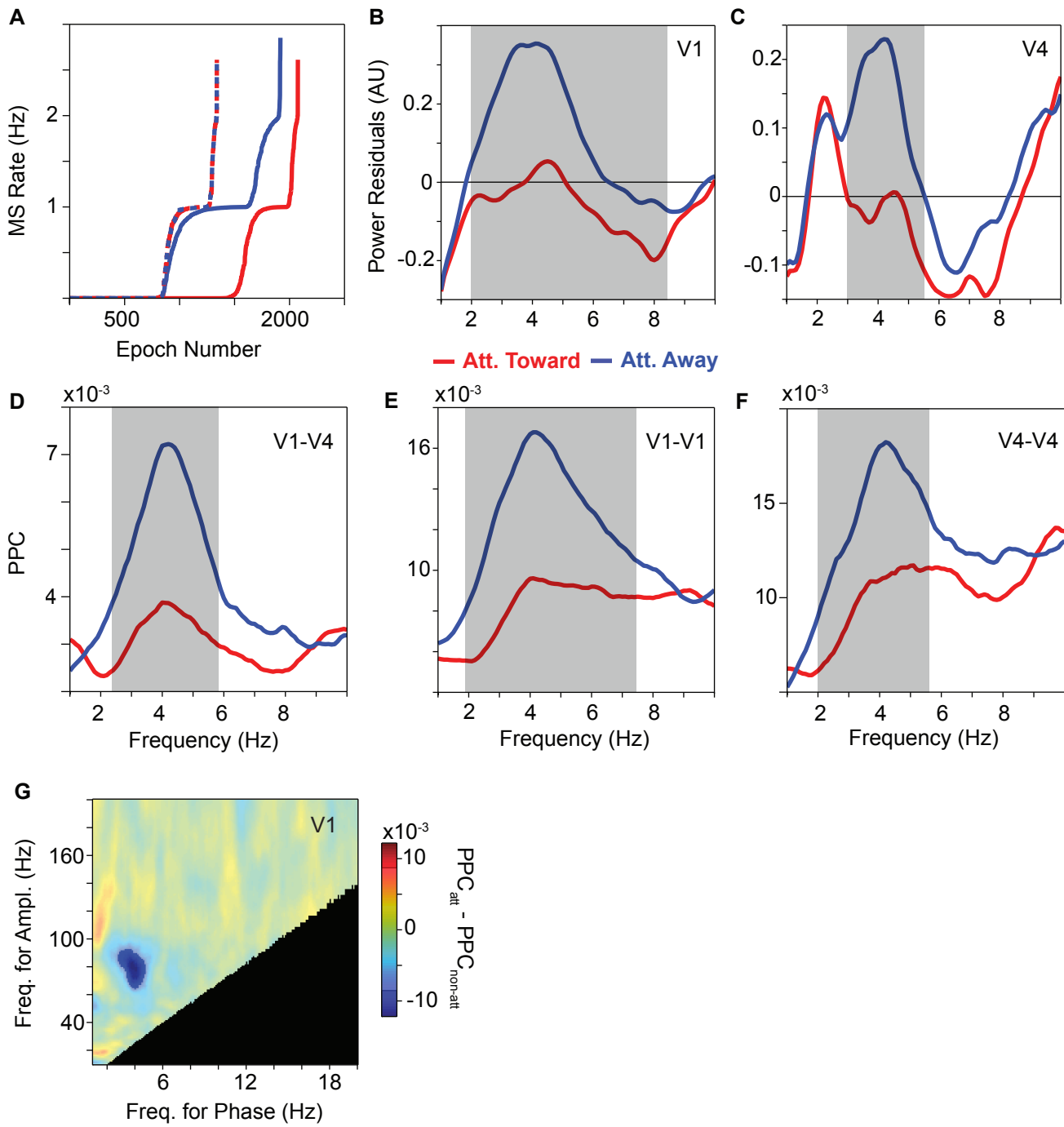


Figure 9  
Spyropoulos et al.

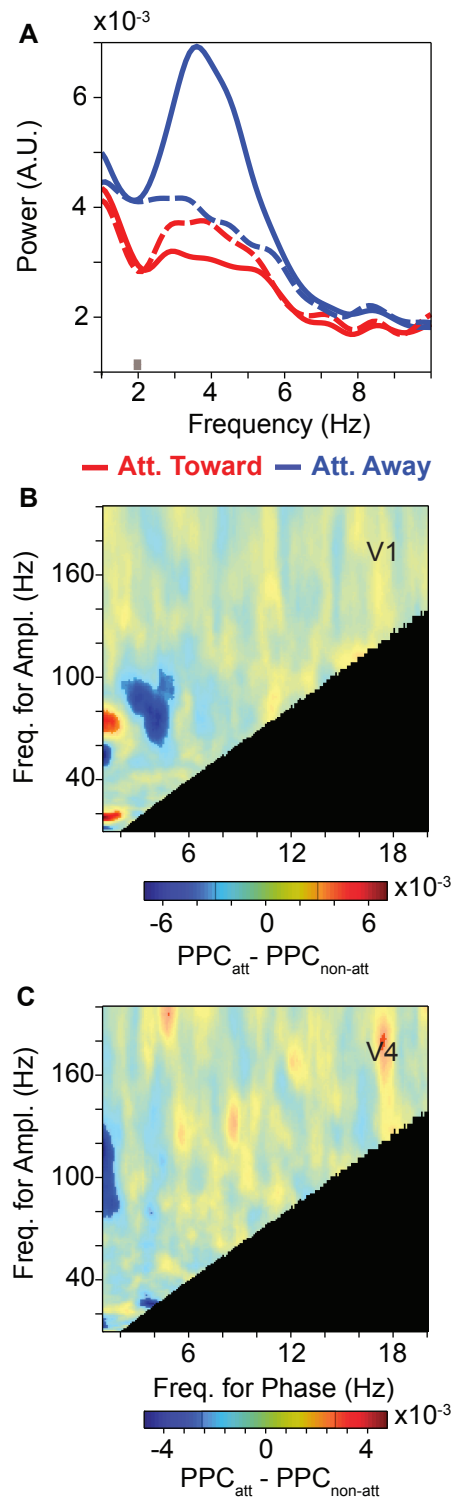


Figure 10  
Spyropoulos et al.